Electrospray synthesis and in-situ sizing of nanoparticulate CsH₂PO₄

Áron Varga¹, Andrew J. Downard², Vanessa Evoen², Konstantinos P. Giapis², Richard C. Flagan², Sossina M. Haile⁴

¹Materials Science, California Institute of Technology, 1200 E. California Blvd., Pasadena, CA 91125, USA

²Chemical Engineering, California Institute of Technology, 1200 E. California Blvd, Pasadena, CA 91125, USA

³Materials Science and Engineering, Northwestern University, 2220 Campus Drive., Evanston, IL 60208, USA

ABSTRACT

Nanometer-sized particles of the solid acid electrolyte material CsH_2PO_4 have been prepared by electrospray synthesis. Using a differential mobility analyzer to provide real-time particle-size information, the role of electrospray parameters, such as precursor solution composition, surface tension, and conductivity, sheath gas temperature and flow rate, and solution flow rate, were evaluated. The results are compared with particle sizes calculated using well-established scaling laws. The much smaller sizes of the detected particles in comparison to the sizes expected from the predicted initial droplet sizes suggests that droplets undergo fission along the path towards deposition. In flight fission events may also explain the observed counterintuitive result that aerosol particle size decreases with increasing solvent concentration. The in situ feedback provided by this system enabled rapid identification of solution and process parameters that result in mean particle sizes of ~ 15 nm, substantially smaller than any prior results.

KEYWORDS

Solid acid fuel cell, electrospray, differential mobility analyzer, nanoparticles, cesium dihydrogen phosphate

1 INTRODUCTION

Fuel cells have long held the promise of efficient, clean, and silent conversion of chemical to electrical energy. As such, they are positioned to play an important role in a sustainable energy future. Among the various types of fuel cells, solid acid fuel cells (SAFCs) incorporating CsH₂PO₄ as the electrolyte are particularly attractive due to their intermediate temperature of operation (~240° C) and the truly solid nature of the proton conducting electrolyte (Boysen et al. 2004; Uda and Haile 2005). These features engender fuel flexibility, enhance impurity tolerance, eliminate fuel cross-over, and obviate challenges with catalyst flooding (Chisholm et al. 2009; Papandrew et al. 2015; Uda et al. 2006). Despite such advantages, state-of-the-art SAFCs deliver lower power densities than their solid oxide fuel cell (SOFC) and polymer electrolyte membrane (PEM) fuel cell counterparts, largely due to performance limitations at the cathode (Chisholm et al. 2009) (Haile et al. 2007). This component is generally constructed as a composite of the electrolyte material, serving as the proton transport medium, and nanoparticulate platinum, serving as the electrocatalyst. Due to the ready oxidation of standard carbon electronic conductors, Pt serves both as electrocatalyst and electron transport medium in the cathode of SAFCs (Chisholm et al. 2009; Lim et al. 2018; Papandrew et al. 2011). Significantly, it has been shown that the cathode overpotential scales with the size of the electrolyte particles in the electrode structure, a phenomenon that has been attributed to the increase in the density of electrocatalytically active triple phase boundaries between the catalyst, the electrolyte, and the gas phase, as the electrolyte particle size decreases (Chisholm et al. 2009). Such an observation motivates an effort to substantially lower the electrolyte particle size while maintaining an interconnected, porous structure.

Accordingly, we have developed spray deposition methods for the preparation of nanostructured SAFC electrodes (Radacsi et al. 2018; Suryaprakash et al. 2014; Varga et al. 2010). Using a commercial spray drier and solutions of CsH₂PO₄ in methanol-water mixtures, it was possible to achieve electrolyte particles as small as 180 nm in diameter as recorded by post-deposition electron microscopy (Suryaprakash et al. 2014). However, the results did not point to any obvious pathways for further decreases in particle size as the limits available from varying the accessible process parameters appeared to have been obtained. The electrospray approach, which combines droplet spraying with the action of an electric field to generate smaller droplets than

attainable by spraying alone (Rulison and Flagan 1994), has proven particularly promising. In a study focused on demonstrating the methodology, particle sizes of ~ 300 nm were readily achieved, again using solutions of CsH₂PO₄ in methanol-water mixtures and again as observed by post-deposition imaging (Varga et al. 2010). Because of the rapid coarsening of the deposited structures (with high particle concentration compared to the conventionally sprayed material) and the sensitivity of the coarsening behavior to laboratory conditions, efforts were focused on the role of additives in stabilizing the structure rather than a systematic study of process parameters. With the simultaneous incorporation of Pt black and the polymer polyvinylpyrrolidone (PVP), feature sizes of ~ 100 nm with good stability were attained. The approach enabled a dramatic reduction in Pt loading in SAFC anodes without sacrifice in the global hydrogen electrooxidation rate. With extremely high polymer content, it was possible to generate a self-supporting fibrous structure with spontaneously formed, isolated CsH₂PO₄ particles approximately ~ 75 nm in diameter, but these rapidly grew to > 150 nm upon exposure to humidity (Radacsi et al. 2018). The fine feature sizes resulted in gains in the oxygen reduction reaction rate relative to standard cathode formulations.

The present work is aimed at preparing CsH_2PO_4 particles even smaller than the ~ 75 nm achieved to date, as a precursor to the creation of cathodes with enhanced activity. A major challenge in the utilization and optimization of the electrospray approach, as currently implemented, is the long development time involved in the deposit-image-modify cycle (Wang et al. 2022). In addition, because of the hygroscopic nature of the electrolyte, it is not known whether the feature sizes recorded post-deposition are reflective of the actual particle size achieved during synthesis or reflect those of the structure in which post-deposition agglomeration has occurred (Radacsi et al. 2018; Varga et al. 2010). In all cases, attaining feature sizes \leq 100 nm by electrospray required the use of various additives (*i.e.*, Pt black, Pt on graphite, carbon nanotubes, or various polymers) which likely arrested such agglomeration.

Here we address the challenges associated with post-deposition characterization through the implementation of *in situ* characterization capabilities. Specifically, we integrate a differential mobility analyzer (DMA) (Flagan 2014) into the electrospray apparatus so as to gain immediate feedback connecting electrospray parameters and aerosol size. A handful of previous studies have demonstrated the benefits of combining electrospray atomization and particle sizing, including for example, studies focused on establishing charged droplet dynamics (Hogan, Biswas and Chen

2009). The integrated system employed here enables a rapid systematic exploration of the parameter space for controlling the electrospray outcome. The parameter space includes solute concentration, which impacts both the surface tension and conductivity of the liquid. These properties (surface tension and conductivity) are independently measured as functions of solute concentration and solvent composition here to facilitate an understanding of the influence of solution chemistry on particle size. The parameter space also includes temperature, which dramatically influences droplet evaporation rate, but over the narrow range examined, has negligible influence on solution properties. The experimentally measured particles sizes are then compared with the scaling law expectations predicted from an analysis presented by Gañán-Calvo (Gañán-Calvo 2004).

2 SOLUTION CHARACTERIZATION

2.1 Methods

The electrolyte CsH₂PO₄ was synthesized from aqueous solution as described elsewhere (Louie, Sasaki and Haile 2008). In brief, stoichiometric quantities of Cs₂CO₃ (Alfa Aesar, 99% metal basis, Stk# 12 887) and H₃PO₄ (Mallinckrodt Chemicals, 85%, Stk#2788-14) were dissolved in deionized water and the precipitation of the compound was induced by introduction of methanol (EMDMillipore, HPLC grade, Stk#67-56-1). Formation of the desired phase was confirmed by X-ray powder diffraction (X'Pert Pro, CuKα, not shown). Polyvinylpyrollidone (PVP, molecular weight 8000, purity), found in our previous work to be effective for morphological stabilization of the resulting structure (Varga et al. 2010), was acquired from a commercial source (Alfa Aesar, Stk# 41626) and used without further purification. Solutions of CsH₂PO₄ and PVP in water-methanol mixtures served as the electrospray liquid, where methanol is introduced to overcome the high surface tension of water and thereby support stable electrospray operation (Borra, Tombette and Ehouarn 1999).

The solubility of CsH₂PO₄ in water-methanol solutions of varied methanol content was determined by a straightforward saturate-and-decant method. An excess of finely ground CsH₂PO₄ was added to the solvent compositions of interest to create saturated solutions. Saturation was ensured by stirring the solutions overnight. Excess solids were allowed to settle by leaving the solutions unstirred for several hours. The dissolved content in the supernatant was determined by

removing 10 mL and measuring the solid mass remaining after the solvent had been fully evaporated (achieved by an overnight hold at 85 °C). Electrical conductivity of the solutions was measured using a digital conductivity meter (Oakton CON 6+). The instrument probe, which was submerged into the solutions for measurement, was cleaned with deionized water between each experiment and recalibrated as necessary to suit the conductivity range of the solutions. The surface tension of selected solutions was measured via the DuNuoy ring method, using a Cenco Interfacial Tensiometer (Precision direct reading model, Ser. No. 909) and a CSC Scientific Inc. platinum ring (Cat. No. 70542, mean circumference 5.992 cm).

2.2 Solution Properties

The solubility limit for CsH₂PO₄ in water methanol mixtures, Figure 1, decreases approximately exponentially with increasing methanol content, from a value of 740 g/L in 90% H₂O to 1.4 g/L in 90 wt% methanol, and undetectable solubility in 100% methanol. In line with this trend, Rashkovich (Rashkovich 1991) reports a solubility of 1500 g/L in 100% H₂O (a condition not explicitly measured here). These solubility values set the limit of the theoretical maximum CsH_2PO_4 concentration that can be employed in the electrospray solutions; it is ≈ 10 g/L at the default methanol content of 67 wt% employed in the electrospray studies. The solution conductivity, Figure 2a, is seen to be highly sensitive to the CsH₂PO₄ concentration and relatively insensitive to the methanol:water ratio. Conversely, the surface tension is almost entirely insensitive to CsH₂PO₄ concentration and strongly sensitive to solvent chemistry, Figure 2b. Both trends are in line with expectations for introducing ions into an aqueous solution and for water/alcohol solutions. Moreover, the measured values for the surface tension of pure distilled water and pure methanol, with values of 73.4 mN/m and 22.5 mN/m, respectively, are in excellent agreement with the literature (Adamson and Gast 1997), as are the measured values for the mixtures thereof. Due to unavoidable solvent evaporation, however, the solute concentration is estimated to have increased by about 10% during the course of each measurement, introducing a small uncertainty in the subsequent analysis of the influence of this parameter. For solutions with 60 wt% methanol, properties measurements were limited to CsH₂PO₄ concentrations of 5 g/L to fully avoid possible complications with solute precipitation. The additive PVP was found to have negligible effect on both the solution conductivity and surface tension, specifically over the

concentration range from 0 to 10 g/L, for solutions with 50 wt% methanol and 3 g/L CsH₂PO₄ (not shown).

3 ELECTROSPRAY PROCEDURES

3.1 Experimental apparatus

Electrospray atomization is a process in which a liquid is supplied to a capillary that is held at a high voltage relative to a substrate placed some distance away from the capillary. Under the influence of the electric field, charged droplets emerging from the capillary migrate towards the substrate. Materials included in the precursor liquid, as either dissolved solutes or suspended particles, can be transported and deposited onto the substrate. Steady emission of droplets is generally preferred for this synthesis approach over erratic emission. In the stable cone-jet mode of droplet emission, a low viscosity liquid adopts a geometry with a conical cusp (the Taylor cone), and a thin jet emerges from the cone tip. Varicose break-up of an axially symmetric jet (in contrast, for example, to whipping break-up in which a jet whips from side to side as droplets are emitted), generates a highly monodisperse distribution of droplets (Cloupeau and Prunetfoch 1994; Hartman et al. 2000b).

The electrospray apparatus constructed for the fabrication of nanoparticulate CsH₂PO₄ has been described previously (Varga et al. 2010). Briefly, the system consists of a heated chamber into which the CsH₂PO₄ solution is supplied by mechanical pumping through an electrically biased stainless steel capillary (ID 127 μm, OD 1.6 mm, *L* 50 mm), Figure 3. The spray is directed upwards, ensuring that any dripping of the solution cannot compromise the quality of the deposited material. For the purposes of *in situ* particle sizing, a grounded collection tube (ID 4.8 mm, OD 20 mm) is placed at the top of the chamber, replacing the grounded holder previously used to secure the particle-collection substrate. Plastic endcaps on either side of the chamber electrically isolate the capillary and the collection tube. A small flow of aerosol is extracted from the electrospray chamber through this tube and directed to a series of instruments for measurement of the particle size (Flagan 2014): a ²¹⁰Po neutralizer, a cylindrical differential mobility analyzer (DMA, TSI Model 3081), and a butanol condensation particle counter (CPC, TSI Model 3010), each described below. The externally controlled deposition parameters are solvent chemistry (i.e., methanol to water ratio), solute concentration, PVP additive concentration, chamber temperature, nitrogen gas

flow rate, liquid supply rate, and tip-to-substrate voltage. The range over which the parameters were varied are indicated in Table 1, as are the default values. For fabrication of fuel cell electrodes, in which the grounded substrate holder is positioned at the mouth of the exhaust tube, the distance from the capillary tip to the holder was fixed in our previous work at 3 cm (Varga et al. 2010). Electron microscopy imaging of the material deposited onto porous carbon paper substrates using the default parameters of Table 1 revealed a CsH₂PO₄ feature size on the order of 300 nm.

As shown in Figure 3, the neutralizer is positioned upstream of the DMA and immediately downstream of the chamber exhaust. By exposing the particles to an electrically neutral cloud of positive and negative gas ions the neutralizer serves to reduce the charge per aerosol particle and to produce a known charge distribution, as required for subsequent sizing. A 210 Po neutralizer was selected as it is particularly efficient for neutralizing aerosols with the charge distribution and flow rates resulting from the electrospray system utilized, though 85 Kr has also been successfully employed for a similar purpose (Kaufman et al. 1996). Within the 210 Po neutralizer environment the aerosol attains a steady-state charge distribution in which a small but known fraction of the particles carries a single elementary unit of charge, *i.e.*, $q = \pm$ e. The positioning of the neutralizer is selected to minimize losses due to electrostatic repulsion and deposition on walls, which could, in turn, influence the measured particle size distribution (Fu et al. 2011). The efficacy of the 210 Po neutralizer was confirmed by measuring the current through an ammeter (Keithley 480 Digital 3.5 Digit Bench Picoammeter) placed in series between the ground wire and the exhaust tube (Varga 2013). With the neutralizer, the current was found to be nearly zero, whereas in the absence of the neutralizer, the current increased linearly with voltage (not shown).

After passing through the neutralizer (beyond which aerosol droplet size decreases only via evaporation of any residual liquid), the polydisperse aerosol is introduced into the cylindrical DMA (flow rate of 0.3 l min⁻¹). A DMA-sheath gas (flow rate of 3 l min⁻¹) is also introduced at the inlet of the DMA. Charged particles entering the DMA are classified according to the velocities with which they migrate across the particle-free sheath-gas flow that is confined between coaxial cylindrical electrodes held at different voltages, indicated highly schematically in Figure 3, with more detailed renditions available in the literature (Flagan 2014). Particles of different diameter are selected by adjusting the electric field strength that is applied transverse to the flow, where the

voltage range is bounded by the electrostatic breakdown at the high end and the onset of diffusional degradation at the low end. Because the drag force is a monotonic function of diameter, singly-charged particles of different sizes follow different trajectories under the influence of the electric field. Those particles whose transit time across the channel equals the residence time in the classification region are eluted in the classified flow. Their mean mobility, Z_p , is simply their velocity (obtained from the residence time and gas space velocity) divided by the mean electric field that they traverse. The remaining particles are rejected in the excess flow or deposited on the walls of the classifier.

The classified aerosol exiting the DMA at each voltage step is then directed to the condensation particle counter (CPC) in which particles are grown by condensation to sufficient size that they can be counted optically. Conducting polymer tubes were used as interconnections in order to avoid parasitic fields arising from charge buildup, which could otherwise cause severe aerosol losses and, hence, bias the recording of the particle size distribution.

The mobility distribution so determined was translated into a size distribution recognizing that the electrophoretic mobility, Z_P , of a spherical particle of diameter d_P and charge q is given by (Camata 1998; Flagan 1999; Stolzenburg and McMurry 2008)

$$Z_{\rm p} = \frac{qC_{\rm c}}{3\pi\mu d_{\rm p}} \tag{1}$$

where C_c is the slip correction factor which accounts for non-continuum effects (a known function of d_p) and μ is the viscosity of the gas. The charge on the particles is taken from the known distribution resulting from the ²¹⁰Po neutralizer. To establish whether the neutralization was sufficient, the residual charge carried by the aerosol particles was measured via a grounded probe and a picoammeter (Keithley 480) placed downstream of the ²¹⁰Po neutralizer.

The particle size distribution data were analyzed using the following standard methodology (Stolzenburg and McMurry 2008). The DMA voltage was measured between 84 V and 500 V in 40 logarithmically spaced steps. At the operating flow rates, this corresponds to a particle size range from 10 to 100 nm. Periodically, a wider particle size range was scanned with voltages ranging from 84 V to 5.2 kV (215 logarithmically spaced steps), extending the size range to 500 nm. The measurement time was 10 sec at each step, with the concentration recorded every second, *i.e.* 10 measurements per step. The transients between the size steps were deleted and the

concentration data for each size step averaged and adjusted for aerosol particle-size-dependent charging statistics described by Hoppel & Frick (Hoppel and Frick 1986) and manufacturer specified counting efficiency of the CPC. The raw data (counts vs. applied voltage) were inverted to obtain the size distribution for each electrospray condition using the methodology proposed by Stolzenburg & McMurry (Stolzenburg and McMurry 2008). The resulting distribution, an example of which is shown in Figure 4 for a fixed set of process parameters, was subsequently parameterized according to a log-normal function - the standard distribution function for dilute nanometer sized aerosol particles. From the analysis the geometric mean diameter, d_g , and standard deviation of the distribution were obtained. The latter are shown as error bars in figures in which the mean sizes are reported. In all cases a single peak was observed in the distribution function, with an undetectably low concentration of particles greater than 100 nm in size. The system was calibrated using polystyrene latex spheres (21, 59, 82, 92, 105 nm diameter, Nanosphere Size Standards, Duke Scientific Corp.) dispersed in de-ionized water and aerosolized via a standard particle aerosolizer (Liu and KW 1975).

3.2 Anticipating the influence of process parameters

There have been extensive studies in the literature, both theoretical and experimental, to understand the relationship between electrospray parameters and the size of the droplets obtained in the varicose break-up regime (Cloupeau and Prunetfoch 1989; 1990; 1994; Gañán-Calvo, Davila and Barrero 1997; Gañán-Calvo 2004; Pantano, Ganan-Calvo and Barrero 1994). Gañán-Calvo has presented a unified analysis that coalesces previous observations of different scaling laws under different experimental regimes (Gañán-Calvo 2004). Under conditions relevant to the present work [(i) inertial forces dominate the jet development over surface tension and viscous forces, and (ii) electrostatic suction dominates over polarization forces in cone-jet necking], the jet diameter, d_i , is given as (Gañán-Calvo 2004)

$$d_{\rm j} = \left(\frac{\rho_{\rm liq}\varepsilon_0}{\gamma_{\rm g-l}K_{\rm liq}}\right)^{1/6} Q^{\nu_2} \tag{2}$$

where ρ_{liq} is the liquid density, K_{liq} is the liquid electrical conductivity, Q is the liquid flow rate, γ_{g-1} is the gas-liquid surface tension, ε_0 is the permittivity of vacuum. Even where polarization forces may dominate cone-jet necking, as is possible for a high dielectric constant liquid, the jet

diameter follows the above expression. The insensitivity to viscosity in this parametric regime implies that the diameter of emitted droplets, d_d , is comparable to that of the jet, and thus d_i can, to a first approximation be evaluated as a proxy for d_d (Cloupeau and Prunetfoch 1994). Others have suggested d_d is on the order of $\frac{1}{4}$ of d_i (Merrill, Pogue and Baucom 2015) and yet others have found that the emitted droplets display a bimodal size distribution, via a process in which secondary droplets with diameter approximately half that of the primary droplets alternate in emission from the jet with the primary droplets (Hartman et al. 1999). For the range of solution parameters explored, Equation (2) implies that the initial primary droplet size is on the order of 1.4 µm and the volume of CsH₂PO₄ dissolved would have a solid diameter on the order of 200 nm. The measured particle diameters, Figure 4, are substantially smaller than given by this analysis, even accounting for a factor of 4 difference between d_d and d_i (Merrill, Pogue and Baucom 2015) or a factor of 2 for secondary droplets (Hartman et al. 1999). If the measured particles are taken to result from simple drying of initial primary droplets, these must have emerged with a size of 170 nm. While not out of the range for electrospray processes, it is small relative to typical observations (Gomez and Tang 1994). This size discrepancy as well as the monomodal particle size distribution, suggest though certainly do not prove, that droplet diminution during flight controls the ultimate particle size.

The charge carried by emitted (primary) droplets is typically ~80% of that corresponding to the Rayleigh limit, the condition at which the electrostatic forces due to the charge on the droplet surface that pull the droplet apart are balanced by the surface forces that pull the droplet together (Gomez and Tang 1994). This limit is expressed as

$$q^2 = 8\pi^2 \varepsilon_0 \gamma_{\underline{q},\underline{1}} d_{\mathrm{d}}^3 \tag{3}$$

where q is the total charge on the droplet, and implies for the present case, a charge per droplet on the order of 10^{-14} C. Complete treatment of the evolution of the velocity and size distributions of charged droplets during travel to the substrate under the force of the macroscopic electric field requires evaluation of a complex set of interactions resulting from droplet-droplet repulsive forces, solvent evaporation, and gas flow dynamics (Arumugham-Achari, Grifoll and Rosell-Llompart 2015; Gañán-Calvo et al. 1994). Broadly described, solvent evaporation results in an increase in the surface charge density of all droplets, while smaller droplets additionally segregate towards the edges of the spray due to differences in drag, electric, and inertial forces on small and large

droplets (Hartman et al. 1999). As in the case of droplet emission from the jet, the Columbic repulsion due to charge concentration resulting from droplet shrinkage from evaporation ultimately overcomes surface tension forces, causing the droplet to undergo a fission event. At this stage, multiple small secondary (or progeny) droplets, which carry 4-40% of the charge, but a much smaller portion of the mass, in some cases < 1 %, are emitted (Dole et al. 1968; Duft et al. 2003; Gu et al. 2007; Hanozin et al. 2023; Hartman et al. 2000b; Smith, Flagan and Beauchamp 2002). Applied to the present studies, first generation (1 mass %) progeny from parent droplets $\approx 1.5 \mu m$ in diameter would generate residual solid particles $\approx 45 \text{ nm}$ in size, very similar to the mean size of 41 nm reported in Figure 4. While the fission process is complex with a continuum of pathways, particularly from submicron ($\sim 100 \text{ nm}$) sized parent droplets (Hanozin et al. 2023), Hunter and Ray (Hunter and Ray 2009) have shown both theoretically and experimentally (in a study exploring the role of liquid surface conductivity) that the diameter of the progeny droplets obtained from parents sized several micrometers is independent of parent droplet size and can be described by

$$d_{p,d} = \alpha \left(\frac{\varepsilon_{liq}}{K_{liq}} \sqrt{\frac{\gamma_{g-l}}{\rho_{liq}}} \right)^{\frac{2}{3}}$$
 (4)

where α is a constant ranging in value from 0.8 to 1.2 and a_{iq} is the dielectric constant of the liquid. This relationship yields values for progeny droplet sizes in the present work that are too small to be physically plausible (< 1 nm), but the scaling laws it embodies can suggest interpretations of observed trends. Beyond causing a reduction in droplet size, the fission process increases the particle size distribution through the repeated generation of progeny, where each distribution is less monodisperse than the prior distribution (Gomez and Tang 1994). The absence of a secondary peak at large sizes in the distribution shown in Figure 4, indicates that if the hypothesis that the detected particles derive from progeny droplets is correct, then the number of residue particles deriving from the parent droplets is undetectably low.

Of particular importance to the synthesis of solid particles by the electrospray process is the question of whether solvent evaporation is complete by the time of deposition. Evaporation dynamics in the present system are extremely complex (multi-component liquid, particle-particle interactions, large heat of vaporization, fission events, appearance of non-continuum effects as the droplet size approaches the mean free path of the gas molecules, *etc.*), and a complete analysis is

beyond the scope of this work. A preliminary evaluation of the evaporation behavior of a single droplet, in a model detailed elsewhere (Evoen 2016), suggested a solvent evaporation time of no more than ~ 5 ms. The analysis was performed assuming an initial droplet diameter of 1 μ m and relative humidity of 1% (obtained from a comparison of the inlet liquid flow rate and the sheath gas flow rate) and accounted for non-continuum effects as well as the decrease in droplet surface temperature due to the heat of vaporization.

Whether the flight time for the droplet/particle to migrate from the capillary tip to the sizer exceeds the < 5 ms evaporation time is not entirely clear because the velocity profile of the droplet (i.e., the initial value and its temporal evolution) is not known. Under the assumption that, at any point in time, including that at the point of ejection, the motion of the charged droplets balances electrostatic and drag forces, the velocity of the droplet relative to the gas-space velocity, $v_{\rm rel}$, is given by (Flagan 2014)

$$v_{rel} = Z_p E \approx \frac{qE}{3\pi\mu d_p} \tag{5}$$

where E is the magnitude of the electric field and the approximation ignores the second-order, non-continuum effects. For an initial droplet diameter of 1 to 3 µm, and an electric field of 1.7×10^5 V m⁻¹ (a typical value employed here) and an initial charge of $\sim 10^{-14}$ C (Eq.), $v_{\rm rel}$ is 5 to 8 m s⁻¹. This value exceeds by many times the gas space velocity of 1.8×10^{-2} m s⁻¹ used in this work, and hence the latter can be ignored. If one then assumes that the relationship between charge and droplet diameter implied by the Rayleigh limit, Eq. , is approximately obeyed by the droplets through each fission step, then the velocity scales with diameter according to $d_d^{v_3}$. The velocity thus decreases monotonically as the droplet size decreases, and the initial (maximum) velocity provides a lower bound on the flight time. For a travel distance of $\sim 3 \times 10^{-2}$ m to the point of deposition where a substrate would be placed, the initial velocity implies a minimum flight time of 4 to 6 ms. This is comparable to the estimated drying time. Thus, it is not possible to determine a priori whether the particles resulting from the parent droplets retain residual solvent upon reaching the substrate for deposition. On the other hand, the progeny particles, which by definition form prior to droplet contact with the substrate, are anticipated to be fully dry due to their very small size.

During flight beyond the position of the grounded collection tube, the particles are no longer under the influence of the electric field and their velocity quickly equilibrates to that of the gas flow (Flagan 2014). Thus, the flight time in this region is protracted, and the likelihood of complete solvent evaporation by the time of particle detection in the DMA is substantially increased. However, given the many approximations utilized in estimating velocity and solvent evaporation rate, generation of an aerosol composed entirely of fully dry particles is not guaranteed.

It becomes evident from this overview that the particle size which ultimately results from electrospray synthesis depends on both solution properties and process parameters (Dole et al. 1968; Hartman et al. 2000a; Pantano, Ganan-Calvo and Barrero 1994). Furthermore, while the Ganan-Calvo expression of Eq. (1), can provide guidance on these dependencies, the expression is unlikely to provide a quantitative prediction of the electrospray process outcome, which includes not only initial droplet formation, but also the complex evolution of the charged droplet into a neutral, and ideally dry, particle deposited onto a conductive substrate. Some authors have developed sophisticated computational approaches using Lagrangian formalisms to describe the evolution of particle dynamics, taking into account the stochastic distribution of initial particle sizes, the influence of gas flow and electric fields, the impact of solvent evaporation, and particleparticle repulsion (Arumugham-Achari, Grifoll and Rosell-Llompart 2015; Gañán-Calvo et al. 1994; Hartman et al. 1999), whereas others, more focused on optimizing the process for desired outcomes, have implemented machine learning approaches to guide selection of process parameters (Wang et al. 2022). Integration of an in situ aerosol sizing tool to evaluate particle size prior to deposition, as implemented here, enables quantitative assessment of the role of the tunable parameters by deconvoluting post-deposition microstructural evolution from the outcome of the droplet generation and particle creation steps.

3.3 Experimental parameter variations

Both solution properties and process parameters were varied as a means of creating small particles, specifically, CsH₂PO₄ concentration, methanol to water ratio, PVP concentration, chamber temperature, nitrogen flow rate, and precursor solution flow rate. Given the breadth of the parameter space, the problem was parsed by retaining a set of default parameters and changing only one variable at a time, Table 1. This default parameter set had been determined in a previous

study to be adequate for deposition of porous solid acid fuel cell electrode structures. (Varga et al. 2010) The full particle size distribution was measured at least two times for each given set of parameters and the results were found to be reproducible, as shown in Figure 4, but in some cases differences in mean particle diameter of a few nm (< 5 nm) was detected for measurements performed on different days. These slight variations are attributed to slight differences in solution composition, which has a strong impact on solution conductivity (Figure 2a). The range of parameter space accessible (in particular the voltage and precursor liquid flow rate) was limited to those conditions that yielded a stable Taylor cone-jet spraying mode. The stability and axisymmetric nature of the spray were monitored by visual observation through the viewing port of the apparatus. Erratic fluctuations in the Taylor cone were interpreted as indications that other spraying modes, such as the multijet, pulsating, or dripping mode, had emerged (Jaworek and Krupota 1999), and such conditions were avoided. Taylor cone instabilities are also reflected in increases in the breadth of the particle size distribution (Chen, Pui and Kaufman 1995).

4 RESULTS AND DISCUSSION

The expected variation in initial droplet size and in corresponding solid volume, computed on the basis of Eq. (2), are shown in Figure 5 as a function of methanol concentration, liquid flow rate, and CsH₂PO₄ concentration. Overall, an initial droplet size in the range of 1 to 3 µm is predicted for the range of conditions explored, with predicted residue particles from these droplets ranging in size from 125 to 425 nm. Variations in methanol content and liquid flow rate at constant solute concentration are predicted to produce variations in dry particle size that scale exactly with the initial droplet size due to simple mass balance relations. Increasing the methanol concentration, Figure 6a, is predicted to induce a moderate increase in the initial droplet size due to the concomitant decrease in conductivity and surface tension, Figure 2; each factor into d_i with a power law dependence of only -1/6, Eq. (2). Increasing the liquid flow rate is predicted to increase the initial droplet size more strongly, Figure 6b, due to the ½ power law exponent for this term in Eq. (2). Increasing the CsH₂PO₄ concentration is anticipated to give rise to a more complex response, Figure 6c. The initial droplet size is predicted to decrease as the solute concentration is increased, largely as a result of an increase in solution conductivity, Figure 2a, while surface tension remains approximately constant, Figure 2b. However, because each droplet would now carry a greater mass of CsH₂PO₄, the residue particle size is predicted to behave oppositely, increasing with increasing

solute concentration. While these predictions suggest approaches for controlling the particle size, the complexity of the droplet ejection, drying, and fission processes, which are unlikely to be captured by the simple relationships presented in Figure 5, motivates the present in situ study to directly observe the impact of process parameters. Indeed, the observed particle sizes reported in Figure 5, which are much smaller than any of the predictions in Figure 5, indicate the limitations of the analytical predictions.

The experimentally measured particle sizes, resulting from variations in methanol concentration, liquid flow rate, and CsH_2PO_4 concentration are summarized Figure 6. Methanol concentration has minimal impact on the final aerosol particle size, Figure 6a, with possibly a shallow minimum at intermediate concentrations. In contrast, as presented in Figure 5a, the initial droplet size is predicted to increase monotonically with methanol content in the solvent, rising by about 15% over the range of compositions examined. More significant than the discrepancy in the trends is again the much smaller particle size, ~ 25 nm, than anticipated (150-200 nm, Figure 5a) based on the prediction of the size of the initially ejected droplets, further suggesting the importance of progeny droplets. A decrease in the liquid flow rate, Figure 5b, results in a decrease in the particle size, as generally expected. However, the impact is substantially smaller than that predicted for the change in initial droplet size ($\sim 50\%$ observed vs. \sim factor of 2.3 predicted for the initial droplet). In addition, high flow rates cause the spray to become somewhat unstable, resulting in broad particle size distributions.

In contrast to the first two parameters, the impact of solute concentration on the particle size is rather strong, Figure 6c. Increasing the CsH₂PO₄ concentration causes a clear decrease in particle size along with a distinct narrowing of the particle size distribution. At the default CsH₂PO₄ concentration to 10 g/L, the experimentally measured mean particle size is about 25 nm, and the size rises to almost 50 nm when the solute concentration is decreased to 0.5 g/L. The decrease in particle size with increasing solute concentration occurs despite the increase in solids content of the initial droplets, which otherwise predicts an increase in residue particle size, Figure 6c. This behavior can plausibly be explained by a strong reduction in the size of the progeny droplets as a result of the increased solution conductivity, Eq. (4). The three-fold increase in conductivity over the CsH₂PO₄ concentration range explored, Figure 2, would result in a factor of two decrease in progeny droplet size, a stronger influence than on the initial droplet size. Moreover, solvent evaporation likely renders the solution from which progeny are emitted more conductive

than the parent solution, amplifying the impact of initial solute concentration on particle size. In contrast to the results obtained here, a more intuitive trend of increasing particle size with increasing solute concentration has been observed in spray drying of CsH₂PO₄ in the absence of an electric field (Suryaprakash et al. 2014). Regardless of the detailed mechanism, the observation of a particle size that decreases rather than increases with solute concentration strongly implies that the detected residue particles derive largely from progeny rather than parent droplets. As alluded to above, such behavior would explain the overall observation of aerosol particles much smaller than those predicted by Eq. (2). While the circumstantial evidence of progeny formation is strong, direct experimental observations are required to draw decisive mechanistic conclusions.

The influence of four additional parameters, ones for which model predictions are not available, are shown in Figures 7. Of these, the most impactful is temperature (Figure 8a). Increasing the chamber temperature would be expected to substantially increase the solvent evaporation rate, but the means by which evaporation rate impacts final particle size is not entirely obvious. One possibility is that the particle retains solvent (in varying amounts) all the way through the end of the flightpath. This could explain the initial decrease in size with increasing temperature, but not the increase in size at high temperature. More significantly, as discussed above, it is likely the particles are fully dry before they enter the CPC. Prior to neutralization and in the period during which solvent remains, an increase in evaporation rate would be expected to increase the frequency of Coulomb fission events. However, according to the study of Hunter and Ray (2009) and articulated in Eq. (4), the progeny droplet size is independent of the number of fission events and would not be affected without a concomitant change in solution properties. The solution properties were not measured as a function of temperature. As a surrogate, reported trends in the properties of water - dielectric constant (Malmberg and Maryott 1956), electrical conductivity (Ageev and Rybin 2020), surface tension (Patek, Souckova and Klomfar 2016), and density (Jones and Harris 1992),— were used to evaluate the possible impact of temperature on $d_{p,d}$. Specifically, the measured properties were taken to vary with temperature according the behavior of neat water. The analysis suggests a 40% decrease in progeny size with an increase in temperature from 20 to 80 °C (the approximate boiling point of the methanol-water mixture, excluding the effect of the solute), consistent with the observed decrease in measured particle size from 32 to 16 nm over this approximate temperature range. The increase in particle size beyond ~ 80 °C, however, cannot be explained by the properties of the solution. We suggest that at these chamber temperatures, rapid evaporation of the solvent generates hollow particles of enlarged diameter (Messing, Zhang and Jayanthi 1993) as are commonly observed in high temperature spray drying processes (Bertling, Blomer and Kummel 2004). Such an outcome would be possible here if solvent is retained just beyond the neutralizer, and the droplet dries via solid precipitation over its surface followed by solvent permeation through the solid shell. We have previously observed hollow particles (with direct microstructural confirmation) in the case of conventionally spray-dried CsH₂PO₄ (Suryaprakash et al. 2014). Significant for the use of CsH₂PO₄ in electrochemical technologies are the very small sizes possible upon controlling temperature. Under optimal conditions, the mean particle size is just 15 nm, a size that has not been achieved by any other method. In our previous electrospray study (Varga et al. 2010), in which characterization of post-deposition structures was limited to SEM observation, not only were the feature sizes much larger than measured here, but also the important temperature effect was not detected. We attribute those earlier outcomes to the short flight pathlength, in which case all deposits collected on the substrate likely retained residual solvent (rather than all being fully dry). Additionally, post-deposition coarsening of the structure may have occurred prior to imaging.

The absence of measurable impact from the other three parameters, nitrogen flow rate, electrospray voltage, and PVP concentration, provides flexibility in system operation, though reasonable control of the electric field is required. At the lower end of the range in flow rate explored, a broad particle size distribution was obtained, in conjunction with instability of the spray and the emergence of a dripping mode. At the higher end of the range, the particle size distribution is narrow, but corona discharge and/or occasional dielectric breakdown were observed.

As noted above, earlier electrospray synthesis experiments using the default conditions of Table 1 and in which the capillary to substrate distance was ~ 3 cm displayed a mean feature size of ~ 300 nm (Varga et al. 2010), substantially larger than the 25 nm size measured here under nominally identical process conditions and using an identical solution. We suggest that distinct outcomes may result from the following differences between the prior deposition studies and the present *in situ* sizing studies. (1) Due to insufficient drying time, the particles reaching the substrate were likely larger, with limited opportunity to undergo fission, (2) they likely retained residual solvent, and (3) the deposited particles likely underwent agglomeration and coarsening, either as a result of the residual solvent or simply due to the hygroscopic nature of CsH₂PO₄.

5 SUMMARY AND CONCLUSIONS

In situ aerosol size measurement via a differential mobility particle sizer has allowed the characterization of the electrospray parameter space for CsH₂PO₄ nanoparticle synthesis. The recorded sizes, being substantially smaller than the predicted sizes of residue particles from droplets emerging from the Taylor cone, suggests that the residues of progeny droplets were detected. Of the many solution and process parameters explored, chamber temperature and solution concentration have emerged as the most important for controlling ultimate particle size. With increasing chamber temperature, particle size first decreases then rises over the range examined. The behavior is consistent with a process dominated by solvent evaporation effects, and suggests that a long flight path is essential for achieving small particles. The observation that, beyond some threshold, increasing temperature causes increases in particle size suggests that increasing the rate of evaporation is less effective than increasing the evaporation time for attaining nanoparticulate CsH₂PO₄.

An intriguing observation in this work is the reduction of particle size with increasing solute concentration. While the diameter of the initially ejected droplets is predicted to slightly decrease as solute concentration is increased, the solids content of such droplets would increase. Thus, initial droplet size cannot be the controlling factor in setting the size of the detected aerosol particles. Given the long pathlength, we propose that droplet fission occurs, releasing progeny with substantially smaller dimensions than the parent droplet, and that these progeny, being much more numerous that the parent particles from which they emerge, dominate the particle distribution. As solution conductivity (which increases with solute concentration), impacts the size of progeny droplets more strongly than it impacts size of the initial droplets, it is plausible that the size of the progeny droplet residue can decrease with increasing solute concentration. Overall, the very small particle size detected at the particle sizer, much smaller than the size implied from the predicted initial droplet size and the solution concentration, strongly suggests that droplet fission plays a decisive role in the overall process, presumably occurring before the aerosol enters the neutralizer. While the proposals presented here are consistent with the experimental observations, additional studies are required to fully verify these hypotheses. From the perspective of scaled up production, an increase in solution concentration provides the added benefit of an increase in deposition rate.

In sum, the experimental identification of the important process parameters that control aerosol size: solute concentration, chamber temperature, and sheath gas flow rate, and the evidence suggesting incomplete solvent evaporation in prior experiments (Varga et al. 2010), lay down the foundations of a path towards synthesis of nanoscale CsH₂PO₄-based structures with feature size in the 10-15 nm range, a result with potentially dramatic impact in solid acid fuel cell technology. In contrast, spray drying in the absence of an electric field has produced CsH₂PO₄ particles only as small as ~180 nm (Suryaprakash et al. 2014). Within the parameter space explored, chamber temperature emerges as a critical variable, and further iterative tuning against all the process and solution parameters (which was not systematically pursued here) has the potential to lower the particle size even further. With particle size targets reached, commercial scale-up will require attention to throughput and morphological stabilization of the nominally uncoated particles.

6 ACKNOWLEDGEMENTS

This work was funded through the generous support of the Resnick Sustainability Institute (California Institute of Technology) and the Ver Steeg Faculty Fellowship Program (Northwestern University). Additional support was provided by the National Science Foundation via award DMR 2118201. The authors thank Hyung Wan Do for assistance in performing sizing experiments, Berhanu (Hanu) Snyder for rendering Figure 3, and Andrew Green for validation of solubility limits, under the supervision of Dylan Bardgett, whose contributions are also gratefully acknowledged.

Table 1. Parameters varied in the electrospray deposition process. The sprayed solution consists of CsH₂PO₄ dissolved in a water-methanol mixture, in some cases with PVP added as a surfactant. Reported methanol content is the mass % in the solvent phase only.

	Methanol (wt %)	CsH ₂ PO ₄ (g/L)	PVP (g/L)	Temperature (°C)	N ₂ flow rate (cm ³ /min)	Liq flow rate* (ml/h)	Voltage* (kV)
Range	33 - 67	0.5 - 10	1 - 30	22 - 120	200 - 1200	0.5 - 2.5	4.9 - 5.75
Default	67	5 or 10	1	100	1000	0.5	5

^{*}The voltage and liquid flow rate settings cannot be varied entirely independently as they are restricted to values that yield a stable Taylor cone and constant particle concentration.

Figure Captions

Figure 1. Solubility limit of CsH₂PO₄ in water-methanol mixtures. Five conditions were measured twice (with some datapoints being visually indistinguishable in the figure), from which the average, standard deviation was found to be 9%. Star datapoint is taken from Rashkovich (1991) and is not included in the linear fit shown as the dotted line.

Figure 2. Properties of water-methanol-CsH₂PO₄ solutions as a function of solute concentration at selected methanol (MeOH) concentrations, given as weight % in the solvent: (a) conductivity; and (b) surface tension. Insets show trends with methanol content, at selected CsH₂PO₄ concentrations in (a) and in the absence of CsH₂PO₄ in (b). To fully avoid possible complications due to solute precipitation, data were not collected close to the solubility limit.

Figure 3. Schematic of the apparatus used for electrospray synthesis of CsH₂PO₄ nanoparticles and the *in situ* sizing thereof. HV is high voltage.

Figure 4. Measurement of CsH₂PO₄ particle diameter distribution at a representative set of conditions (Table 1): (a) counts as a function of particle diameter at discrete sizes over multiple measurements; and (b) averaged values (from two separate measurement campaigns) along with fit to a single log-normal distribution. Width of the distribution is reported as the error bar in Figures 6 and 7.

Figure 5. Predicted droplet sizes based on Eq. (2), and size of the corresponding solid residue particle: (a) as a function of methanol content with dissolved CsH₂PO₄ concentration fixed at 10 g/L and liquid flow rate fixed at 0.5 mL/h; (b) as a function of liquid flow rate with methanol content fixed at 60 wt% of the solvent and dissolved CsH₂PO₄ concentration fixed at 10 mL/g; and (c) as a function of dissolved CsH₂PO₄ concentration with methanol content fixed at 60 wt% of the solvent and liquid flow rate fixed at 0.5 mL/h.

Figure 6. Influence of selected parameters on the measured aerosol particle size from electrospray synthesis of CsH₂PO₄: (a) methanol concentration in the solvent phase; (b) liquid flow rate; and (c) CsH₂PO₄ concentration. Where not varied, the methanol content in the solvent phase is 67 wt%, the CsH₂PO₄ concentration is 10 g/L, and liquid flow rate is 0.5 mL/h. In all

cases, the chamber temperature is 100 °C, the nitrogen sheath gas flow rate is 1000 cm 3 /min, the solution contains 1 g/L of PVP, and the tip-to-substrate voltage is ~ 5 kV.

Figure 7. Influence of selected parameters on the measured aerosol particle size from electrospray synthesis of CsH_2PO_4 : (a) chamber temperature; (b) nitrogen sheath gas flow rate; and (c) tip-to-substrate voltage; and (d) PVP concentration. Where not varied, the chamber temperature is 100 °C, the nitrogen sheath gas flow rate is 1000 cm³/min, the electrospray voltage is ~ 5 kV, and the PVP concentration is 1 g/L. In all cases, the methanol content in the solvent phase is 67 wt%, the liquid flow rate is 0.5 mL/h, and the CsH_2PO_4 concentration is 10 g/L.

References

- Adamson, A. W. and A. P. Gast. 1997. *Physical chemistry of surfaces*. New York: John Wiley & Sons, Inc.
- Ageev, I. M. and Y. M. Rybin. 2020. Features of measuring the electrical conductivity of distilled water in contact with air. *Meas. Tech.* 62:923-927. doi: 10.1007/s11018-020-01714-2.
- Arumugham-Achari, A. K., J. Grifoll, J. Rosell-Llompart. 2015. A comprehensive framework for the numerical simulation of evaporating electrosprays. *Aerosol Science and Technology* 49:436-448. doi: 10.1080/02786826.2015.1039639.
- Bertling, J., J. Blomer, R. Kummel. 2004. Hollow microspheres. *Chem. Eng. Technol.* 27:829-837. doi: 10.1002/ceat.200406138.
- Borra, J. P., Y. Tombette, P. Ehouarn. 1999. Influence of electric field profile and polarity on the mode of ehda related to electric discharge regimes. *Journal of Aerosol Science* 30:913-925. doi: 10.1016/S0021-8502(98)00779-4.
- Boysen, D. A., T. Uda, C. R. I. Chisholm, S. M. Haile. 2004. High-performance solid acid fuel cells through humidity stabilization. *Science* 303:68-70. doi: 10.1126/Science.1090920.
- Camata, R. P. 1998. Aerosol synthesis and characterization of silicon nanocrystals: California Institute of Technology.
- Chen, D., D. Pui, S. Kaufman. 1995. Electrospraying of conducting liquids for monodisperse aerosol generation in the 4 nm to 1.8 um diamater range. *Journal of Aerosol Science* 26:963-977. doi.
- Chisholm, C. R. I., D. A. Boysen, A. B. Papandrew, S. Zezevic, S. Cha, K. Sasaki, A. Varga, K. P. Giapis, S. M. Haile. 2009. From laboratory curiosities to technological realization: The development path for solid acid fuel cells. *Interface Magazine* 18:53-59. doi.
- Cloupeau, M. and B. Prunetfoch. 1989. Electrostatic spraying of liquids in cone-jet mode. *J Electrostat* 22:135-159. doi: 10.1016/0304-3886(89)90081-8.
- Cloupeau, M. and B. Prunetfoch. 1990. Electrostatic spraying of liquids main functioning modes. *J Electrostat* 25:165-184. doi: 10.1016/0304-3886(90)90025-Q.

- Cloupeau, M. and B. Prunetfoch. 1994. Electrohydrodynamic spraying functioning modes a critical-review. *Journal of Aerosol Science* 25:1021-1036. doi: 10.1016/0021-8502(94)90199-6.
- Dole, M., L. Marck, R. Hines, R. Mobley, L. Ferguson, M. Alice. 1968. Molecular beams of macroions. *The Journal of Chemical Physics* 49:2240. doi: 10.1063/1.1670391.
- Duft, D., T. Achtzehn, R. Müller, B. A. Huber, T. Leisner. 2003. Rayleigh jets from levitated microdroplets. *Nature* 421:128-128. doi: 10.1038/421128a.
- Evoen, V. 2016. Electrocatalysis in solid acid fuel cell electrodes: California Institute of Technology.
- Flagan, R. C. 1999. On differential mobility analyzer resolution. *Aerosol Science and Technology* 30:556-570. doi: 10.1080/027868299304417.
- Flagan, R. C. 2014. Continuous-flow differential mobility analysis of nanoparticles and biomolecules, in *Annual review of chemical and biomolecular engineering, vol 5*, Prausnitz, J. M., M. F. Doherty, R. A. Segalman, eds., 255-279. Palo Alto: Annual Reviews.
- Fu, H., A. C. Patel, M. J. Holtzman, D. R. Chen. 2011. A new electrospray aerosol generator with high particle transmission efficiency. *Aerosol science and technology: the journal of the American Association for Aerosol Research* 45:1176-1183. doi: 10.1080/02786826.2011.582899.
- Gañán-Calvo, A., J. Davila, A. Barrero. 1997. Current and doplet size in the electrospraying of liquids scaling laws. *Journal of Aerosol Science* 28:249-275. doi.
- Gañán-Calvo, A. M. 2004. On the general scaling theory for electrospraying. *J Fluid Mech* 507:203-212. doi.
- Gañán-Calvo, A. M., J. C. Lasheras, J. Dávila, A. Barrero. 1994. The electrostatic spray emitted from an electrified conical meniscus. *Journal of Aerosol Science* 25:1121-1142. doi: 10.1016/0021-8502(94)90205-4.
- Gomez, A. and K. Tang. 1994. Charge and fission of droplets in electrostatic sprays. *Physics of Fluids* 6:404. doi: 10.1063/1.868037.
- Gu, W., P. E. Heil, H. Choi, K. Kim. 2007. Comprehensive model for fine coulomb fission of liquid droplets charged to rayleigh limit. *Applied Physics Letters* 91:064104. doi: 10.1063/1.2767774.
- Haile, S. M., C. R. I. Chisholm, K. Sasaki, D. A. Boysen, T. Uda. 2007. Solid acid proton conductors: From laboratory curiosities to fuel cell electrolytes. *Faraday Discussions* 134:17. doi: 10.1039/b604311a.
- Hanozin, E., C. C. Harper, M. S. McPartlan, E. R. Williams. 2023. Dynamics of rayleigh fission processes in ~100 nm charged aqueous nanodrops. *ACS Central Science* 9:1611-1622. doi: 10.1021/acscentsci.3c00323.
- Hartman, R., D. Brunner, D. Camelot, J. Marijnissen, B. Scarlett. 2000a. Jet break-up in electrohydrodynamic atomization in the cone-jet mode. *Journal of Aerosol Science* 31:65-95. doi.

- Hartman, R. P. A., J. P. Borra, D. J. Brunner, J. C. M. Marijnissen, B. Scarlett. 1999. The evolution of electrohydrodynamic sprays produced in the cone-jet mode, a physical model. *J Electrostat* 47:143-170. doi: 10.1016/s0304-3886(99)00034-0.
- Hartman, R. P. A., D. J. Brunner, D. M. A. Camelot, J. C. M. Marijnissen, B. Scarlett. 2000b. Jet break-up in electrohydrodynamic atomization in the cone-jet mode. *Journal of Aerosol Science* 31:65-95. doi.
- Hogan, C. J., P. Biswas, D. R. Chen. 2009. Charged droplet dynamics in the submicrometer size range. *J. Phys. Chem. B* 113:970-976. doi: 10.1021/jp807765n.
- Hoppel, W. A. and G. M. Frick. 1986. Ion—aerosol attachment coefficients and the steady-state charge distribution on aerosols in a bipolar ion environment. *Aerosol Science and Technology* 5:1-21. doi: 10.1080/02786828608959073.
- Hunter, H. C. and A. K. Ray. 2009. On progeny droplets emitted during coulombic fission of charged microdrops. *Physical Chemistry Chemical Physics* 11:6156-6165. doi: 10.1039/B820457H.
- Jaworek, A. and A. Krupota. 1999. Classification of the modes of ehd spraying. *Journal of Aerosol Science* 30:873-893. doi.
- Ji, J. H., G. N. Bae, J. Hwang. 2004. Characteristics of aerosol charge neutralizers for highly charged particles. *Journal of Aerosol Science* 35:1347-1358. doi: 10.1016/j.jaerosci.2004.04.008.
- Jones, F. E. and G. L. Harris. 1992. Its-90 density of water formulation for volumetric standards calibration. *J. Res. Natl. Inst. Stand. Technol.* 97:335-340. doi: 10.6028/jres.097.013.
- Kaufman, S. L., J. W. Skogen, F. D. Dorman, F. Zarrin, K. C. Lewis. 1996. Macromolecule analysis based on electrophoretic mobility in air: Globular proteins. *Anal. Chem.* 68:1895-1904. doi: 10.1021/ac951128f.
- Lim, D. K., J. Liu, S. A. Pandey, H. Paik, C. R. I. Chisholm, J. T. Hupp, S. M. Haile. 2018. Atomic layer deposition of pt@csh2po4 for the cathodes of solid acid fuel cells. *Electrochim. Acta* 288:12-19. doi: 10.1016/j.electacta.2018.07.076.
- Liu, B. and L. KW. 1975. American Industrial Hygene Association 36:861-865. doi.
- Louie, M. W., K. Sasaki, S. M. Haile. 2008. Towards understanding electrocatalysis in cdp based fuel cells pt and pd thin film electrodes. *Electrochemical Society Transactions* 13:57-62. doi.
- Malmberg, C. G. and A. A. Maryott. 1956. Dielectric constant of water from 0-degrees to 100-degrees-c. *J. Res. Natl. Bur. Stand.* 56:1-8. doi: 10.6028/jres.056.001.
- Merrill, M. H., W. R. Pogue, J. N. Baucom. 2015. Electrospray ionization of polymers: Evaporation, drop fission, and deposited particle morphology. *J. Micro Nano-Manuf.* 3:7. doi: 10.1115/1.4028505.
- Messing, G. L., S. C. Zhang, G. V. Jayanthi. 1993. Ceramic powder synthesis by spray-pyrolysis. *J. Am. Ceram. Soc.* 76:2707-2726. doi: 10.1111/j.1151-2916.1993.tb04007.x.
- Pantano, C., A. Ganan-Calvo, A. Barrero. 1994. Zeroth-order electrohydrostatic solution for electrospraying in cone-jet mode. *Journal of Aerosol Science* 25:1065-1077. doi.

- Papandrew, A. B., R. W. Atkinson Iii, R. R. Unocic, T. A. Zawodzinski. 2015. Ruthenium as a cotolerant hydrogen oxidation catalyst for solid acid fuel cells. *Journal of Materials Chemistry A* 3:3984-3987. doi: 10.1039/C4TA06451H.
- Papandrew, A. B., C. R. I. Chisholm, R. A. Elgammal, M. M. Ozer, S. K. Zecevic. 2011. Advanced electrodes for solid acid fuel cells by platinum deposition on csh₂po₄. *Chemistry of Materials* 23:1659-1667. doi: 10.1021/cm101147y.
- Patek, J., M. Souckova, J. Klomfar. 2016. Generation of recommendable values for the surface tension of water using a nonparametric regression. *J. Chem. Eng. Data* 61:928-935. doi: 10.1021/acs.jced.5b00776.
- Radacsi, N., F. D. Campos, C. R. I. Chisholm, K. P. Giapis. 2018. Spontaneous formation of nanoparticles on electrospun nanofibres. *Nat. Commun.* 9:8. doi: 10.1038/s41467-018-07243-5.
- Rashkovich, L. N. 1991. *Kdp-family single crystals*. Bristol, England: Adam Hilger.
- Rulison, A. J. and R. C. Flagan. 1994. Synthesis of yttria powders by electrospray pyrolysis. *J. Am. Ceram. Soc.* 77:3244-3250. doi: 10.1111/j.1151-2916.1994.tb04577.x.
- Smith, J. N., R. Flagan, J. Beauchamp. 2002. Droplet evaporation and discharge dynamics in electrospray ionization. *Journal of Physical Chemistry A* 106:9957-9967. doi.
- Stolzenburg, M. R. and P. H. McMurry. 2008. Equations governing single and tandem dma configurations and a new lognormal approximation to the transfer function. *Aerosol Science and Technology* 42:421-432. doi: 10.1080/02786820802157823.
- Suryaprakash, R. C., F. P. Lohmann, M. Wagner, B. Abel, A. Varga. 2014. Spray drying as a novel and scalable fabrication method for nanostructured csh₂po₄, pt-thin-film composite electrodes for solid acid fuel cells. *RSC Adv.* 4:60429-60436. doi: 10.1039/c4ra10259b.
- Uda, T., D. A. Boysen, C. R. I. Chisholm, S. M. Haile. 2006. Alcohol fuel cells at optimal temperatures. *Electrochem. Solid State Lett.* 9:A261-A264. doi: 10.1149/1.2188069.
- Uda, T. and S. M. Haile. 2005. Thin-membrane solid-acid fuel cell. *Electrochemical and Solid-State Letters* 8:A245. doi: 10.1149/1.1883874.
- Varga, A. 2013. Advancing electrocatalysis in solid acid fuel cell electrodes: California Institute of Technology.
- Varga, Á., N. A. Brunelli, M. W. Louie, K. P. Giapis, S. M. Haile. 2010. Composite nanostructured solid-acid fuel-cell electrodes via electrospray deposition. *J Mater Chem* 20:6309-6315. doi: Doi 10.1039/C0jm00216j.
- Wang, F., M. Elbadawi, S. L. Tsilova, S. Gaisford, A. W. Basit, M. Parhizkar. 2022. Machine learning predicts electrospray particle size. *Materials & Design* 219:110735. doi: 10.1016/j.matdes.2022.110735.

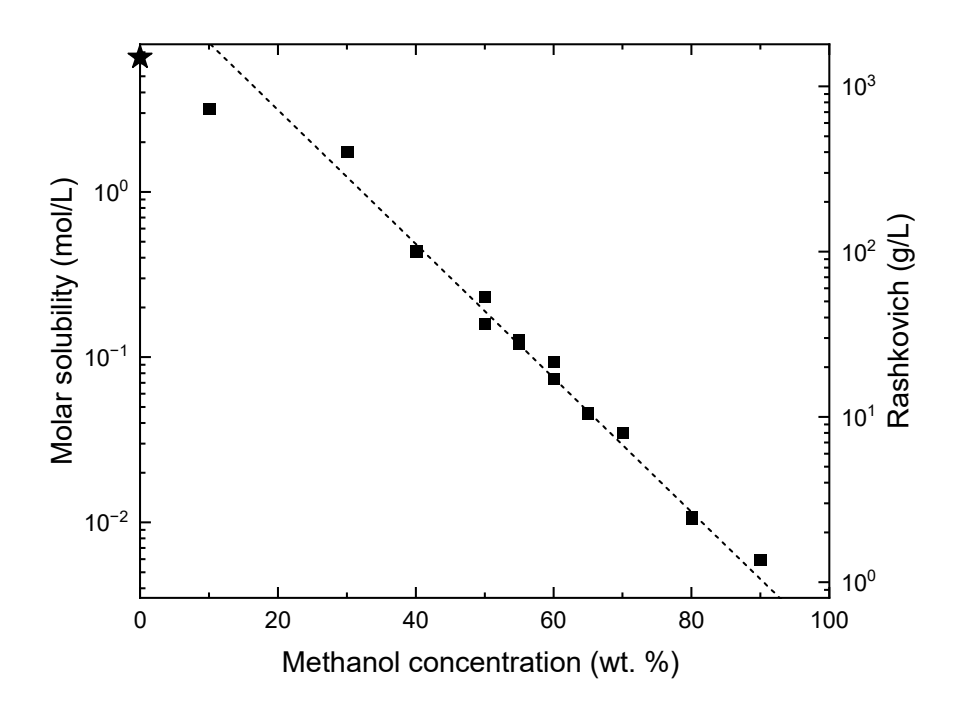


Figure 1. Solubility limit of CsH₂PO₄ in water-methanol mixtures. Five conditions were measured twice (with some datapoints being visually indistinguishable in the figure), from which the average standard deviation was found to be 9%. Star datapoint is taken from Rashkovich and is not included in the linear fit shown as the dotted line.

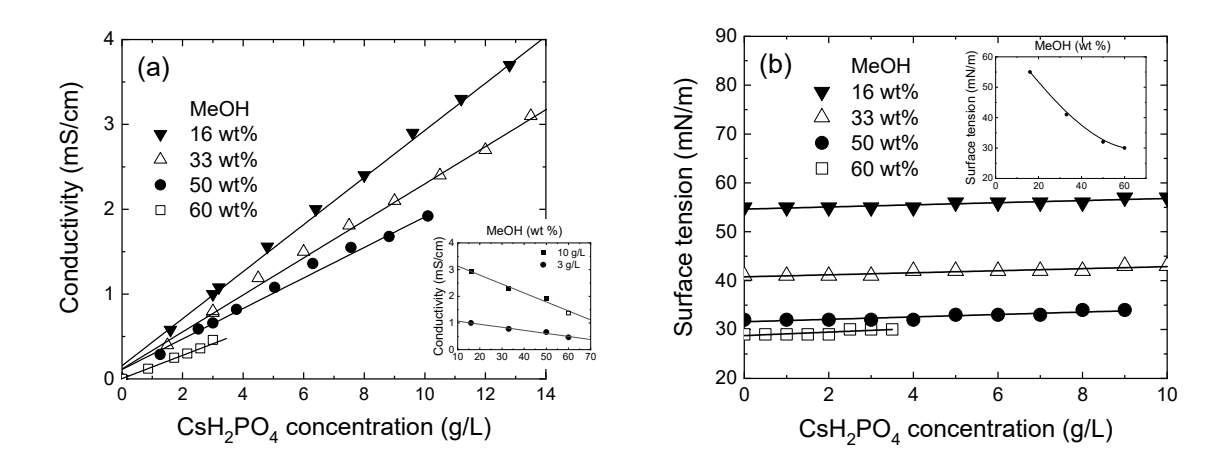


Figure 2. Properties of water-methanol-CsH₂PO₄ solutions as a function of solute concentration at selected methanol (MeOH) concentrations, given as weight % in the solvent: (a) conductivity; and (b) surface tension. Insets show trends with methanol content, at selected CsH₂PO₄ concentrations indicated in (a) and in the absence of CsH₂PO₄ in (b). To fully avoid possible complications due to solute precipitation, data were not collected close to the solubility limit.

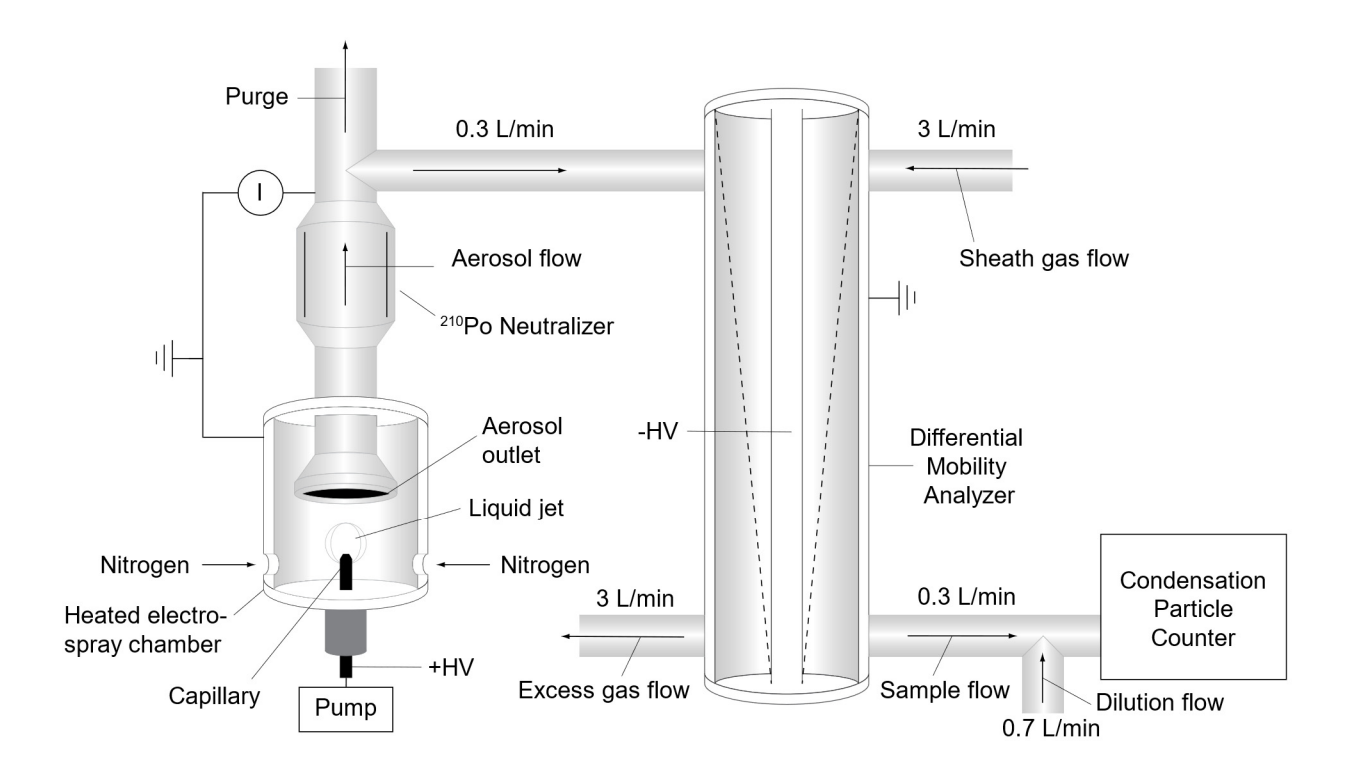


Figure 3. Schematic of the apparatus used for electrospray synthesis of CsH₂PO₄ nanoparticles and the *in situ* sizing thereof. HV is high voltage.

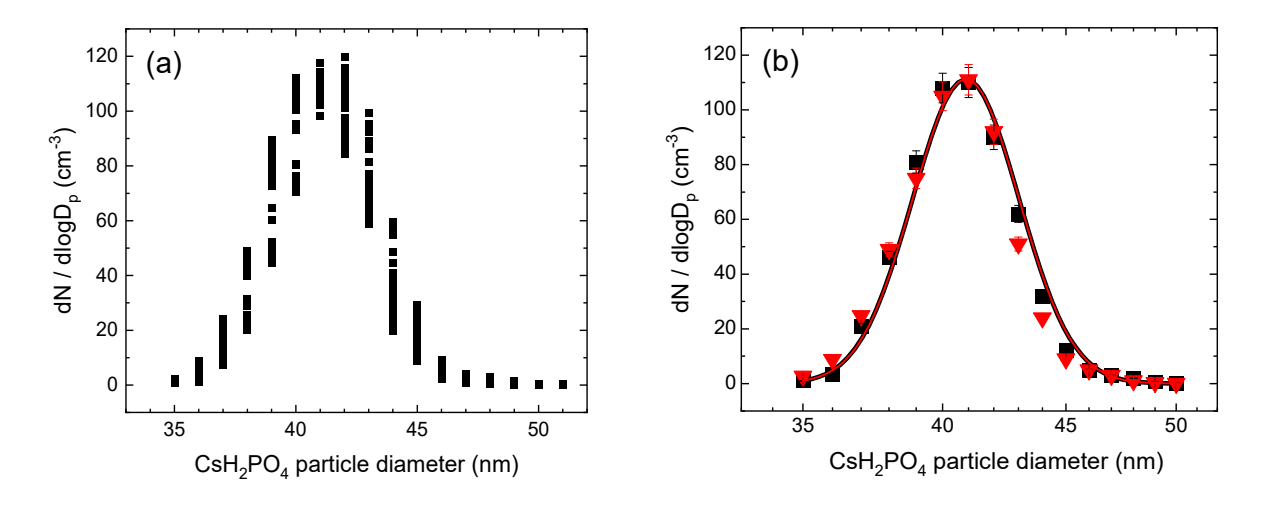


Figure 4. Representative measurement of CsH₂PO₄ particle diameter distribution (a) counts as a function of particle diameter at discrete sizes over multiple measurements; and (b) averaged values (from two separate measurement campaigns) along with fit to a single log-normal distribution. Width of the distribution is reported as the error bar in Figures 6 and 7.

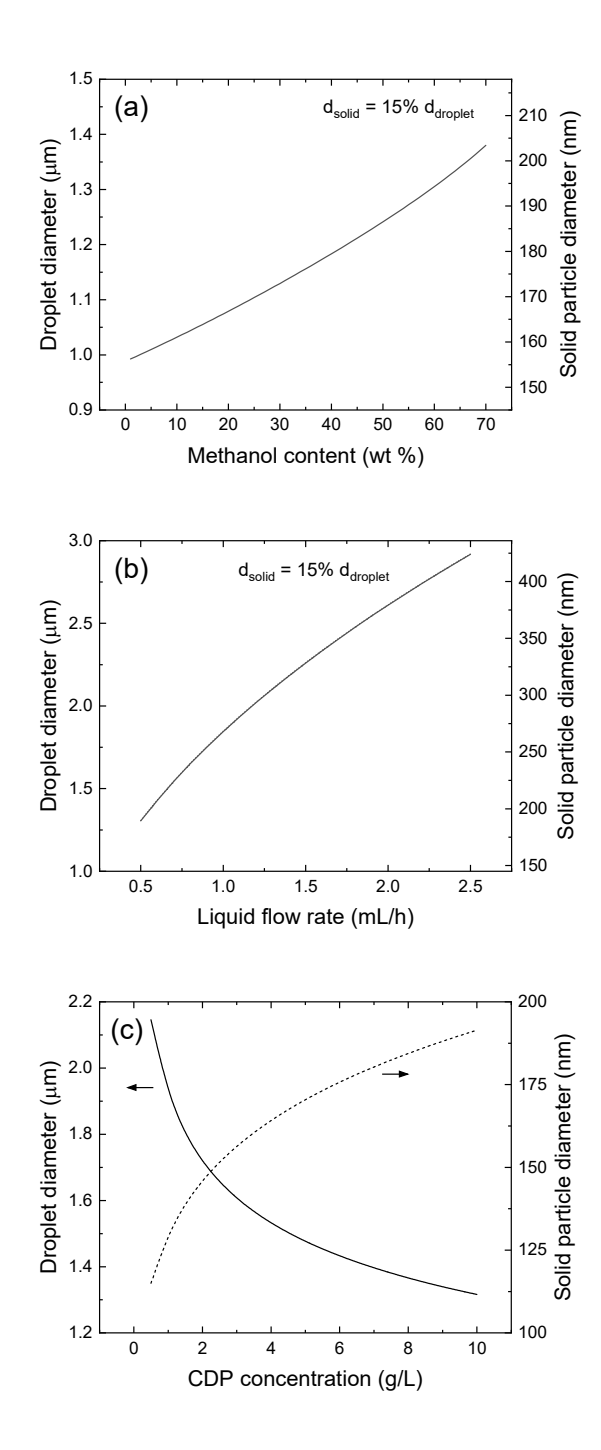


Figure 5. Predicted droplet sizes based on Eq. (2), and size of the corresponding solid residue particle: (a) as a function of methanol content with dissolved CsH_2PO_4 concentration fixed at 10 g/L and liquid flow rate fixed at 0.5 mL/h; (b) as a function of liquid flow rate with methanol content fixed at 60 wt% of the solvent and dissolved CsH_2PO_4 concentration fixed at 10 mL/g; and (c) as a function of dissolved CsH_2PO_4 concentration with methanol content fixed at 60 wt% of the solvent and liquid flow rate fixed at 0.5 mL/h.

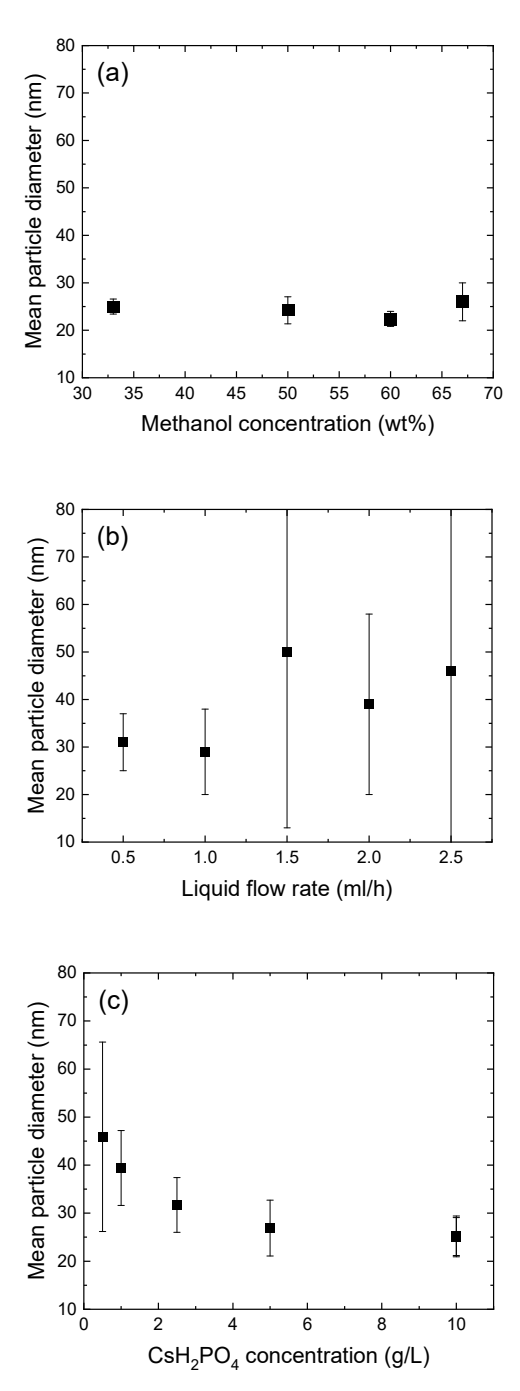


Figure 6. Influence of selected parameters on the measured aerosol particle size from electrospray synthesis of CsH_2PO_4 : (a) methanol concentration in the solvent phase; (b) liquid flow rate; and (c) CsH_2PO_4 concentration. Where not varied, the methanol content in the solvent phase is 67 wt%, the CsH_2PO_4 concentration is 10 g/L, and liquid flow rate is 0.5 mL/h. In all cases, the chamber temperature is 100 °C, the nitrogen sheath gas flow rate is 1000 cm³/min, the solution contains 1 g/L of PVP, and the tip-to-substrate voltage is ~ 5 kV.

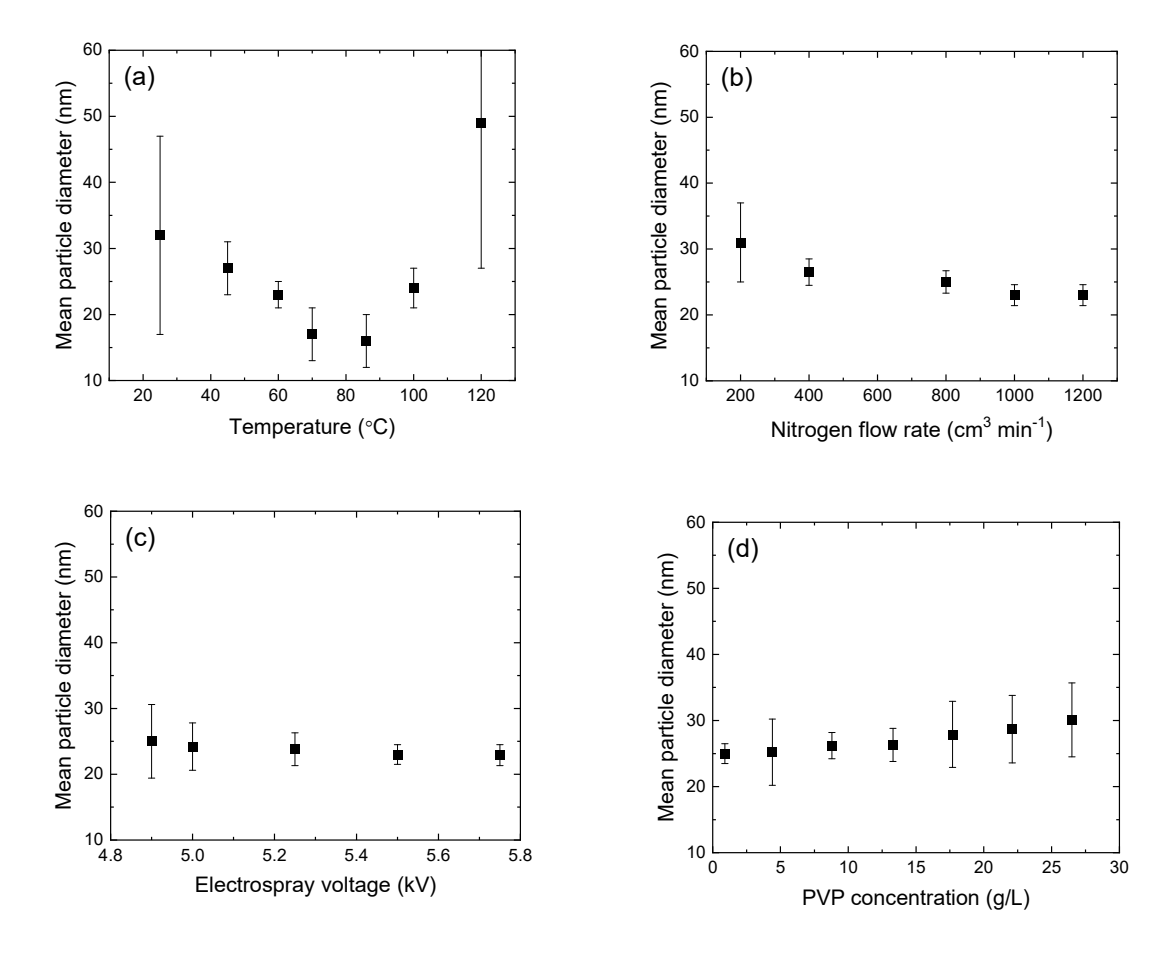


Figure 7. Influence of selected parameters on the measured aerosol particle size from electrospray synthesis of CsH₂PO₄: (a) chamber temperature; (b) nitrogen sheath gas flow rate; and (c) tip-to-substrate voltage; and (d) PVP concentration. Where not varied, the chamber temperature is $100~^{\circ}$ C, the nitrogen sheath gas flow rate is $1000~^{\circ}$ Cmin, the electrospray voltage is $\sim 5~\text{kV}$, and the PVP concentration is 1 g/L. In all cases, the methanol content in the solvent phase is 67~wt%, the liquid flow rate is 0.5~mL/h, and the CsH₂PO₄ concentration is 10~g/L.